Geophys. J. Int. (2007) **168,** 1021–1028 doi: 10.1111/j.1365-246X.2006.03328.x

FAST TRACK PAPER

Global Positioning System measurements of strain accumulation and slip transfer through the restraining bend along the Dead Sea fault system in Lebanon

Francisco Gomez,[1] Gebran Karam,[2] Mohamad Khawlie,[3] Simon McClusky,[4] Philippe Vernant,[4] Robert Reilinger,[4] Rani Jaafar,[1] Charles Tabet,[5] Kamal Khair[6] and Muawia Barazangi[7]

[1] *Department of Geological Sciences, University of Missouri, Columbia, Missouri* 65211. *E-mail: fgomez@missouri.edu*
[2] *Department of Civil Engineering, Lebanese American University, Jbail, Lebanon*
[3] *Lebanese National Center for Remote Sensing, Beirut, Lebanon*
[4] *Department of Earth, Atmospheric, and Planetary Sciences, Massachusetts Institute of Technology, Cambridge, Massachusetts* 02139
[5] *Lebanese National Council for Scientific Research, Beirut, Lebanon*
[6] *Hasbaya, Lebanon*
[7] *Institute for the Study of the Continents, Snee Hall, Cornell University, Ithaca, New York* 14853*, USA*

Accepted 2006 December 19. Received 2006 December 4; in original form 2006 August 7

SUMMARY

Approximately 4 yr of campaign and continuous Global Positioning System (GPS) measurements across the Dead Sea fault system (DSFS) in Lebanon provide direct measurements of interseismic strain accumulation along a 200-km-long restraining bend in this continental transform fault. Late Cenozoic transpression within this restraining bend has maintained more than 3000 m of topography in the Mount Lebanon and Anti-Lebanon ranges. The GPS velocity field indicates 4–5 mm yr^{-1} of relative plate motion is transferred through the restraining bend to the northern continuation of the DSFS in northwestern Syria. Near-field GPS velocities are generally parallel to the major, left-lateral strike-slip faults, suggesting that much of the expected convergence across the restraining bend is likely accommodated by different structures beyond the aperture of the GPS network (e.g. offshore Lebanon and, possibly, the Palmyride fold belt in SW Syria). Hence, these geodetic results suggest a partitioning of crustal deformation involving strike-slip displacements in the interior of the restraining bend, and crustal shortening in the outer part of the restraining bend. Within the uncertainties, the GPS-based rates of fault slip compare well with Holocene-averaged estimates of slip along the two principal strike-slip faults: the Yammouneh and Serghaya faults. Of these two faults, more slip occurs on the Yammouneh fault, which constitutes the primary plate boundary structure between the Arabia and Sinai plates. Hence, the Yammouneh fault is the structural linkage that transfers slip to the northern part of the transform in northwestern Syria. From the perspective of the regional earthquake hazard, the Yammouneh fault is presently locked and accumulating interseismic strain.

Key words: crustal deformation, Dead Sea fault system, fault motion, Global Positioning System (GPS), Neotectonics, transform faults.

INTRODUCTION

The central part of the Dead Sea fault system (DSFS) in Lebanon and southwestern Syria is a ∼200 km long restraining bend that strikes 25°–30° from the main trend of the transform (Fig. 1). Within the geodynamic framework of the eastern Mediterranean region, the left-lateral DSFS is the continental transform boundary between the Arabian and Sinai plates (e.g. Freund *et al.* 1970; McKenzie 1972), accommodating the differential motion of those two plates as they converge and collide with Eurasia.

Although late Cenozoic strike-slip movements of the DSFS are well documented (e.g. Quennell 1958; Freund *et al.* 1970), some debate has persisted over the past decade concerning the present-day activity of the northern DSFS and whether or not plate motion

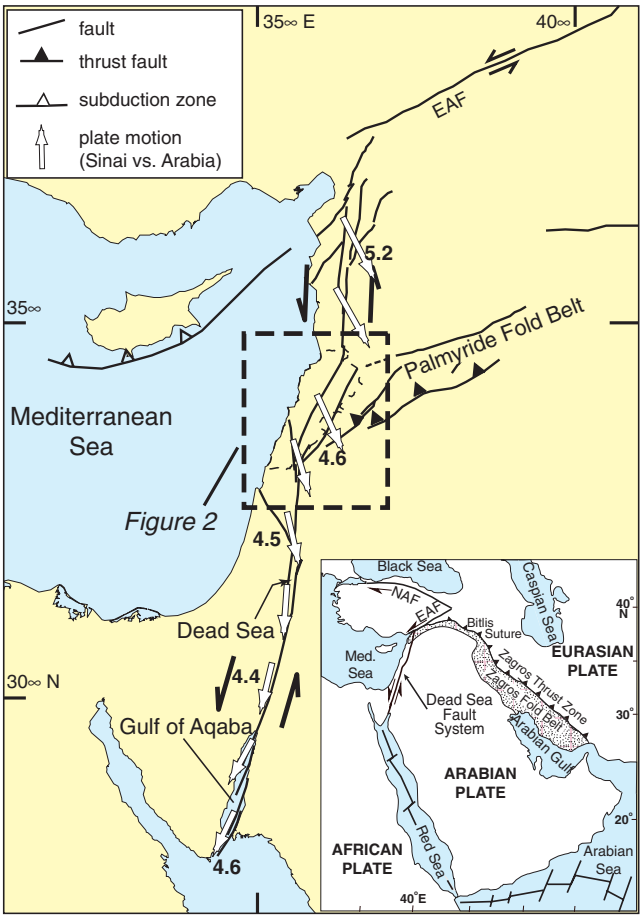

Figure 1. Regional tectonic map of the Dead Sea fault system. Also shown are the relative plate motions (mm yr^{-1}) (Sinai versus Arabia) predicted by Reilinger *et al.* (2006). Abbreviations: EAF = East Anatolian fault and NAF = North Anatolian fault.

is presently transmitted through the restraining bend (Girdler 1990; Butler *et al.* 1998). This debate was motivated, primarily, by the apparent lack of instrumentally recorded seismicity along the restraining bend and the northern portion of the transform in NW Syria. Specific questions concerning the DSFS include: Is strain presently accumulating within the restraining bend? If so, how is crustal deformation distributed? How do short-term (geodetic) estimates of fault slip compare with long-term (late Quaternary) estimates?

Whether or not the central DSFS is an active restraining bend also pertains to broader questions of how large restraining bends in major transcurrent fault systems develop. Faults within restraining bends typically have orientations that are not optimal with regard to the regional plate motions (i.e. the boundary forces). Yet restraining bends persist, often involving increased structural complexity compared with the rest of the fault system.

This 'Lebanese' restraining bend compares in scale to other large restraining bends, such as the Big Bend along the San Andreas fault system in southern California. Late Cenozoic transpression within the Lebanese restraining bend has uplifted the Mount Lebanon and Anti-Lebanon ranges to elevations in excess of 3000 m. Similar to the San Andreas fault system within the Big Bend, the single trace of the southern DSFS splays into several structures within the Lebanese restraining bend (Walley 1988, Fig. 2): the Yammouneh, Serghaya, Rachaya, Roum and Akkar faults. Of those, the Yammouneh fault appears to be the only through-going structure that connects the southern and northern parts of the DSFS. The Serghaya fault, the other major NNE–SSW strike-slip fault, seems to terminate in the northern Anti-Lebanon range (Gomez *et al.* 2003, 2006). Two faults striking oblique to the transform, the Roum fault in the south and the Akkar fault in the north, appear to serve as the structural linkages between the strike-slip faults of the restraining bend and horizontal shortening of the Mount Lebanon range (e.g. Gomez *et al.* 2006; Nemer & Meghraoui 2006).

Geodetic estimates of present-day plate motion along the DSFS are relatively slow at 4–6 mm yr^{-1}. (e.g. Wdowinski *et al.* 2004; Mahmoud *et al.* 2005). This is consistent with longer return periods (500–1000 yr) for strike-slip earthquakes within the Lebanese restraining bend (e.g. Gomez *et al.* 2003; Meghraoui *et al.* 2003; Daeron *et al.* 2005). Despite a general seismic quiescence at the present time, historical records document numerous large earthquakes within the restraining bend, most notably in 551 AD, 1202 AD, 1759 AD and 1837 AD (e.g. Sbeinati *et al.* 2005). Hence, understanding the active crustal deformation, particularly in terms of strain accumulation and the earthquake cycle, is critical to improving the estimates of the regional earthquake hazard.

Recent palaeoseismic and neotectonic studies within the Lebanese restraining bend have helped constrain the late Pleistocene/Holocene kinematics of several major faults: purely strike-slip displacement is documented along the Yammouneh fault (4–6 mm yr^{-1}) and Serghaya fault (1–1.5 mm yr^{-1}) (Gomez *et al.* 2003; Daeron *et al.* 2004; Gomez *et al.* 2007). Along the Roum fault, a strike-slip rate of 1 mm yr^{-1} in the south grades into increased dip slip towards the northern end of the fault (Nemer & Meghraoui 2006).

This study reports the initial, near-field Global Positioning System (GPS) velocity estimates for the Lebanese restraining bend along the DSFS. The results permit kinematic modelling of the restraining bend and quantify the accumulation of interseismic strain along the Yammouneh fault.

GPS MEASUREMENTS AND DATA PROCESSING

The regional GPS network used in this study includes one local continuous GPS station (LAUG) and 14 survey monuments (Fig. 2). Monumentation at the 14 survey sites consisted of 10 cm steel pins cemented into bedrock. Sites were distributed about Lebanon in order to facilitate 2-D analysis of the resulting velocities. The campaign sites were repeatedly measured during five survey campaigns between spring 2002 and fall 2005. In each campaign, sites were observed for a minimum of 24 hr using Trimble 5700 receivers with Zephyr Geodetic antennae atop fixed-height antenna masts in order to reduce uncertainty owing to antenna setup.

GPS data were processed in a two-step procedure using the GAMIT/GLOBK software (Herring *et al.* 1997; Dong *et al.* 1998; King & Bock 1998). In the first step, loosely constrained estimates of station coordinates, orbital and Earth orientation parameters, and atmospheric zenith delays were determined from raw GPS observables using GAMIT. Data from the Lebanon GPS network were analysed along with raw GPS data from other continuously operating GPS stations in the region. Subsequently, a global Kalman filter (GLOBK) was applied to the combined, loosely constrained solutions and their associated covariances in order to estimate a consistent set of station coordinates and velocities. As part of this second step, a six parameter transformation was estimated by minimizing the horizontal velocities of 49 globally distributed IGS stations with respect to the IGS00 realization of the ITRF 2000 no-net-rotation

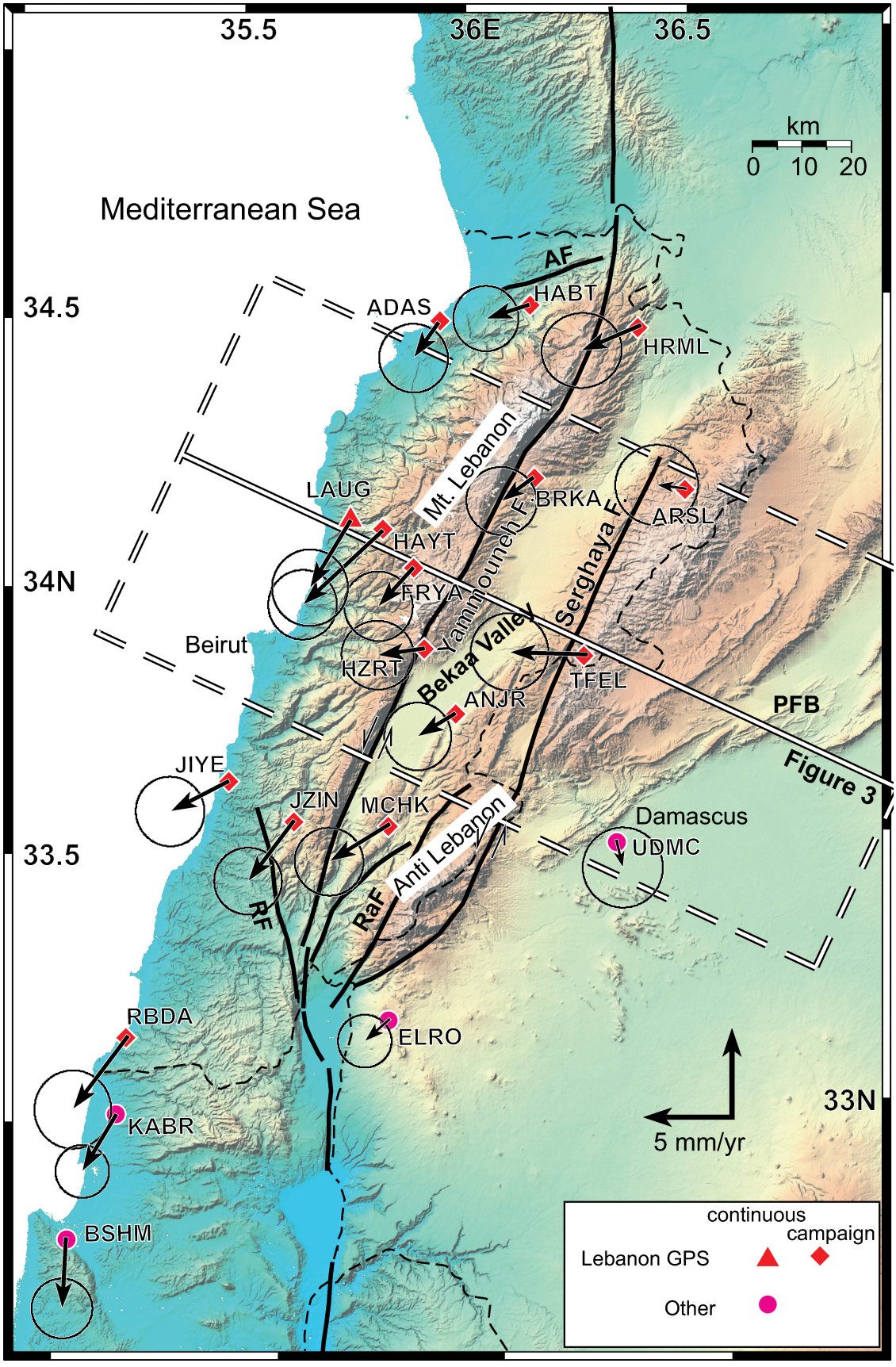

Figure 2. Map showing general structure of the Lebanese restraining bend. GPS velocities for the network used in this study are also shown in an Arabia-fixed reference frame (2σ uncertainties). Abbreviations for some key tectonic features: RF = Roum fault, RaF = Rachaya fault, AF = Akkar fault and PFB = Palmyride fold belt. Box denotes the swath encompassed by the profiles in Fig. 3.

Table 1. Velocities of GPS sites shown in Fig. 2.

			ITRF 2000		Arabia-fixed				
Site	Longitude	Latitude	Vel E	Vel N	Vel E	Vel N	σE	σN	Correlation
Survey sites									
ARSL	36.467	34.164	22.21	5.33	−1.66	0.22	0.94	0.91	0.007
HRML	36.379	34.412	20.37	3.65	−3.33	−1.42	0.91	0.85	0.023
TFEL	36.225	33.860	19.71	5.16	−4.37	0.13	0.88	0.88	−0.004
BRKA	36.143	34.184	22.03	3.66	−1.81	−1.34	0.80	0.77	−0.019
HABT	36.084	34.451	21.22	4.18	−2.43	−0.79	0.74	0.74	−0.003
ANJR	35.922	33.730	22.03	3.63	−2.12	−1.29	0.76	0.77	−0.001
ADAS	35.909	34.466	22.23	2.92	−1.40	−1.99	0.78	0.78	−0.013
HZRT	35.880	33.869	21.43	4.52	−2.63	−0.38	0.82	0.78	−0.011
FRYA	35.829	34.005	21.97	2.70	−1.98	−2.19	0.78	0.79	−0.013
HAYT	35.767	34.094	19.44	0.71	−4.46	−4.15	0.78	0.79	0.002
MCHK	35.771	33.526	20.92	2.76	−3.38	−2.10	0.78	0.77	−0.012
JZIN	35.589	33.555	21.70	1.40	−2.57	−3.40	0.77	0.76	−0.001
JIYE	35.411	33.651	20.90	3.03	−3.29	−1.70	0.78	0.79	−0.012
RBDA	35.162	33.139	21.43	0.55	−3.09	−4.10	0.87	0.89	0.002
Continuous stations									
LAUG	35.674	34.115	21.60	1.06	−2.27	−3.77	0.86	0.87	0.008
UDMC	36.285	33.510	24.69	3.47	0.37	−1.57	0.91	0.91	−0.002
ELRO	35.771	33.182	23.11	3.60	−1.42	−1.26	0.61	0.60	−0.001
KABR	35.145	33.023	22.70	1.45	−1.91	−3.19	0.61	0.60	0.002
BSHM	35.023	32.779	24.56	0.63	−0.21	−3.97	0.69	0.68	0.001

reference (NNR) frame. A 'random walk' noise of 1 mm/$\sqrt{}$ yr was also assumed in the final velocity estimation.

This study focuses on the near-field deformation constrained by repeated GPS survey campaigns and, accordingly, only data from regional stations during the time periods of the GPS survey campaigns were analysed. Previous studies have already presented regional results based on the complete time-series analyses of daily GPS solutions (e.g. Wdowinski *et al.* 2004; Mahmoud *et al.* 2005; Reilinger *et al.* 2006), and these studies have already constrained the regional plate models very well.

After stabilizing the reference frame, the site velocities were resolved to an Arabian-fixed reference frame, which facilitates assessing the local deformation. Velocities (in NNR and Arabia-fixed reference frames) for the sites around the Lebanese restraining bend are provided in Table 1.

RESULTS AND MODELLING

Fig. 2 depicts the resulting velocity field around the Lebanese restraining bend. Uncertainties for the resulting velocities are typically less than 1 mm yr^{-1} (1σ). In the Arabia-fixed reference frame shown in Fig. 2, the sites along the Lebanese coast demonstrate SSW motion of the Sinai plate relative to Arabia. South of the restraining bend, the velocities rotate to a more southward direction, maintaining their fault-parallel orientation.

Within the central part of the restraining bend, velocity variations along a WNW–ESE profile (i.e. perpendicular to the NNE–SSW strike of the Yammouneh and Serghaya faults, see Fig. 2) permit an initial kinematic assessment. The profiles in Fig. 3 decompose the velocities into motions parallel and perpendicular to the Yammouneh and Serghaya faults. These profiles deliberately exclude GPS survey sites at the extremities of the restraining bend and those which might be complicated by the obliquely striking Roum fault. The velocities parallel to the transform (Fig. 3a) show a progressive increase in southward velocity from east to west—a pattern that is generally consistent with basic models of elastic strain accumulation (e.g. Savage & Burford 1973). In addition to this strike-slip deformation, the fault-normal components of displacement (Fig. 3b) suggest up to 2 mm yr^{-1} of motion (i.e. shortening) between sites in the Anti-Lebanon (TFEL and ARSL) and the continuous station along the Lebanese coast (LAUG). This convergence is demonstrated by a consistent trend in all of the Lebanese stations, although UDMC is a clear outlier.

An initial, quantitative assessment of the geodetic slip rate is based on a 1-D elastic dislocation model of a locked fault. Following Savage & Burford (1973), this profile model assumes an infinitely long strike-slip fault and expresses the station velocity, b, as a function of the long-term slip rate (V), fault locking depth (D) and distance from the fault (x):

$$b = (V/\pi)\tan^{-1}(x/D). \quad (1)$$

Owing to the size of the uncertainties relative to the velocities, present observations, warrant only a single fault model (i.e. the Yammouneh fault). Despite the simplifications and assumptions, this analytical model permits assessing a range of values of fault slip rates and locking depths consistent with the GPS data using a grid search. The 1σ contour shown in Fig. 3(c) is based on a Monte Carlo simulation to assess the noise level in the data (e.g. Sandvol & Hearn 1994). As demonstrated in Figs 3(a) and (c), the entire range of geological slip estimates (3.5–6.5 mm yr^{-1}) can be modelled to fit nearly all of the velocities, with locking depths of 8–25 km. As shown in Fig. 3(c), the peak of the probability distribution corresponds with a slip rate of 4.4 mm yr^{-1} and a locking depth of 13 km.

A more appropriate elastic model and robust estimate of the fault slip rate involves 2-D blocks bounded by faults of finite lengths, rather than a 1-D profile. This modelling follows the methodology of Meade & Hager (2005), and considers the spatial variations in the velocity field due to fault geometry, and the effect of block rotations that are not accounted for in 1-D models, and both can significantly impact deduced slip rates. In this approach, an optimal fit between plate motion, fault slip, and GPS velocities is determined using a